A comparative study of state-of-the-art evolutionary image registration methods for 3D modeling ☆

J. Santamaría [a,*], O. Cordón [b,c], S. Damas [b]

[a] Dept. of Computer Science, EPS Linares, University of Jaén, 23700 Linares, Jaén, Spain
[b] European Centre for Soft Computing, Edif. Investigación, Mieres, Asturias, Spain
[c] Dept. of Computer Science and Artificial Intelligence, ETSIIT, University of Granada, Granada, Spain

ARTICLE INFO

ABSTRACT

Image registration (IR) aims to find a transformation between two or more images acquired under different conditions. This problem has been established as a very active research field in computer vision during the last few decades. IR has been applied to a high number of real-world problems ranging from remote sensing to medical imaging, artificial vision, and computer-aided design. Recently, there is an increasing interest on the application of the evolutionary computation paradigm to this field in order to solve the ever recurrent drawbacks of traditional image registration methods as the iterated closest point algorithm. Specially, evolutionary image registration methods have demonstrated their ability as robust approaches to the problem. Unlike classical IR methods, they show the advantage of not requiring a good initial estimation of the image alignment to proceed. In this contribution, we aim to review the state-of-the-art image registration methods that lay their foundations on evolutionary computation. Moreover, we aim to analyze the performance of some of the latter approaches when tackle a challenging real-world application in forensic anthropology, the 3D modeling of forensic objects.

© 2011 Elsevier Inc. All rights reserved.

1. Introduction

Image registration (IR) [1–3] is a fundamental task in computer vision (CV) used to finding either a spatial *transformation* (e.g, rotation, translation, etc.) or a correspondence (matching of similar image features) among two or more images acquired under different conditions: at different times, using different sensors, from different viewpoints, or a combination of them. IR aims to achieve the best possible overlapping transforming those independent images into a common one. Over the years, IR has been applied to tackle many real-world problems ranging from remote sensing to medical imaging, artificial vision, and computer-aided design (CAD). Likewise, different techniques facing the IR problem have been studied resulting in a large body of research. Several recent contributions reviewing the state of the art on IR methods can be found in [1–5].

In a nutshell, IR involves finding the optimal *transformation* achieving the best fitting between typically two *images*, usually called scene and model. They both are related by the said transformation and the degree of resemblance between them is measured by a *similarity metric*. Such transformation estimation is usually formulated as an *optimization* problem solved by an iterative procedure in order to properly explore the search space of candidate solutions to the problem. The optimization process applied by traditional IR methods is highly influenced by image noise, image discretization, and orders of magnitude in the scale of the IR transformation parameters, among other phenomena. Specially, that is the case of the approaches based on the classical iterative closest point (ICP) algorithm [6,7], which are likely to provide incorrect registration transformation estimations. This is due to the fact that those methods are usually prone to be trapped in local minima [8–11] since they assume a rough prealignment of the images typically provided by the user.

After a couple of decades, evolutionary computation (EC) [12] has demonstrated its ability to deal with complex real-world problems in CV and image processing. As an example, several special issues on the topic have been published in international journals in the last few years [13–15]. In particular, evolutionary algorithms (EAs) [12,16] have been successfully applied to tackle IR problems without requiring a good initial estimation of the image alignment. That advantage is mainly motivated by the global optimization nature of evolutionary approaches, which allows them to perform a robust search in complex and ill-defined search spaces.

The first attempts to face the IR problem using EC can be found in the eighties [17]. Since then, evolutionary IR (EIR) has become a very active area and several well-known EAs have been considered to tackle the IR optimization process, causing an outstanding interest [18–28]. Nevertheless, those EIR methods have not been covered by any of the IR surveys existing in the specialized literature. The aim of the current contribution is to bridge that gap in a two-fold manner. On the one hand, by reviewing the extensive literature in EIR. On the other hand, by developing an experimental study on the performance of 12 EIR methods when tackling the 3D modeling of some real-world forensic objects digitized by a laser range scanner.

The structure of this contribution is as follows. Section 2 describes the IR problem. Next, Section 3 describes the key concepts of he EC paradigm, it presents the first EIR methods and it reviews the state-of-the-art EIR methods. Section 4 is devoted to a deep experimental study developed on the said real-world IR application. Finally, some conclusions are drawn in Section 5.

2. Image registration

There is not a universal design for a hypothetical IR method that could be applicable to every real-world application [3]. However, IR methods consist of the following four components:

- Two input **Images** named as *scene* $I_s = \{\vec{p}_1, \vec{p}_2, \ldots, \vec{p}_n\}$ and *model* $I_m = \{\vec{p}'_1, \vec{p}'_2, \ldots, \vec{p}'_m\}$, with $\vec{p}_i$ and $\vec{p}'_j$ being image points.
- A **Registration transformation** *f*, relating the two images. Typically, it is a parametric function.
- A **Similarity metric function** *F*. It aims to measure a qualitative value of closeness or degree of fitting between the transformed scene image, noted by $f(I_s)$, and the model image.
- An **Optimizer**. It is a method that seeks the optimal transformation *f* inside the defined solution search space.

Likewise, an iterative process is often followed (see Fig. 1). It usually finishes when convergence is achieved, i.e., when the similarity metric is bellow a given tolerance threshold. In this work, we focused our attention on the optimizer component which is of crucial importance in the success of any IR method. In particular, two search approaches for optimization have been considered in the IR literature [3]:

- On the one hand, we find the *matching-based* approach, where the optimization problem is intended to look for a set of correspondences of pairs of similar image features. Then, the registration transformation is derived from that set. This is the case of the well-known ICP method [6,7], whose main drawback is its sensitiveness to the initial transformation [8–11]. Thus, ICP usually gets stuck in local optima.
- On the other hand, we find the *parameter-based* IR approach which directly explores the values in the range of each transformation parameters.

A detailed description of the IR framework is out of the scope of this contribution. We refer the interested reader to [1–3]. Likewise, the formulation of the IR problem is dependent on the particular environment it is involved (remote sensing, medical imaging, CAD, etc.). Thus, in order to provide a more specific description of the problem, we focused our attention on the particular application we consider in our experiments: the IR of range images for 3D modeling [5,29–31].

Range scanners are able to capture 3D images, named range images, of the surface of the sensed object. Every range image is acquired from a particular viewpoint and it models the geometry of the scanned object partially. Thus, it is mandatory to consider a reconstruction technique to perform the accurate integration of the images in order to achieve a complete and reliable model of the physical object. This framework is usually called 3D modeling (see Fig. 2) and it is based on applying IR techniques to achieve the integration of the range images [5,29–31].

The 3D model reconstruction procedure involves several pair-wise alignments of two adjacent range images in order to obtain the final 3D model of the physical object. Therefore, every pair-wise IR method aims to find the Euclidean motion that brings the *scene* view (I_s) into the best possible alignment with the *model* view (I_m). It is usually considered an Euclidean motion based on a 3D rigid transformation (f) determined by seven real-coded parameters, that is: a rotation $R = (\theta, Axis_x, Axis_y, Axis_z)$ and a translation $\vec{t} = (t_x, t_y, t_z)$, with θ and *Axis* being the angle and axis of rotation, respectively. Then, the transformed points of the *scene* view are denoted by

$$f(\vec{p}_i) = R(\vec{p}_i) + \vec{t}, \ i = 1 \cdots N_{I_s} \tag{1}$$

Hence, the pair-wise IR task can be formulated as an optimization problem developed to search for the Euclidean transformation f^* achieving the best alignment of both images according to the considered *similarity metric F*:

$$f^* = \arg\min_f \ F(I_s, I_m; f) \ s.t. : \ f^*(I_s) \cong I_m \tag{2}$$

The median square error (MedSE) is usually considered the similarity metric in 3D modeling [28,30]:

$$F(I_s, I_m; f) = MedSE(d_i), \ \forall i \in \{1, \ldots, N_{I_s}\} \tag{3}$$

where $MedSE()$ corresponds to the median d_i value. We define $d_i = \|f(\vec{p}_i) - \vec{q}_{cl}\|^2$ as the squared Euclidean distance between the transformed scene point, $f(\vec{p}_i)$, and its corresponding closest point, $\vec{q}_{cl}$, in the *model* view I_m.

In order to speed up the computation of the closest point q_{cl} of I_m, indexing structures as kd-trees [32] or the grid closest point (GCP) transform proposed in [33] are often used. We will consider the GCP scheme in the experimental study (Section 4). In addition, we will follow a feature-based IR approach [3]. Such approaches consider a feature extraction procedure as a preprocessing step, previous to the application of the IR method. They are based on the selection of a small subset of truly representative characteristics of the images to be registered. In previous works [28,34–36], it has been demonstrated that using such IR approach offers a fast and a reliable IR result when range images are considered. In
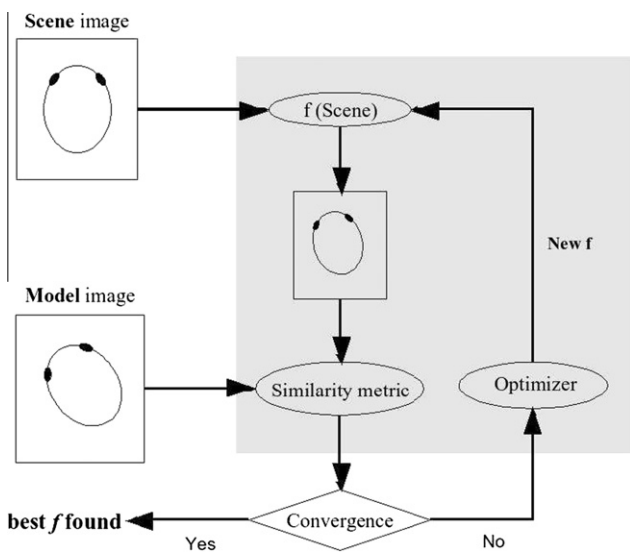

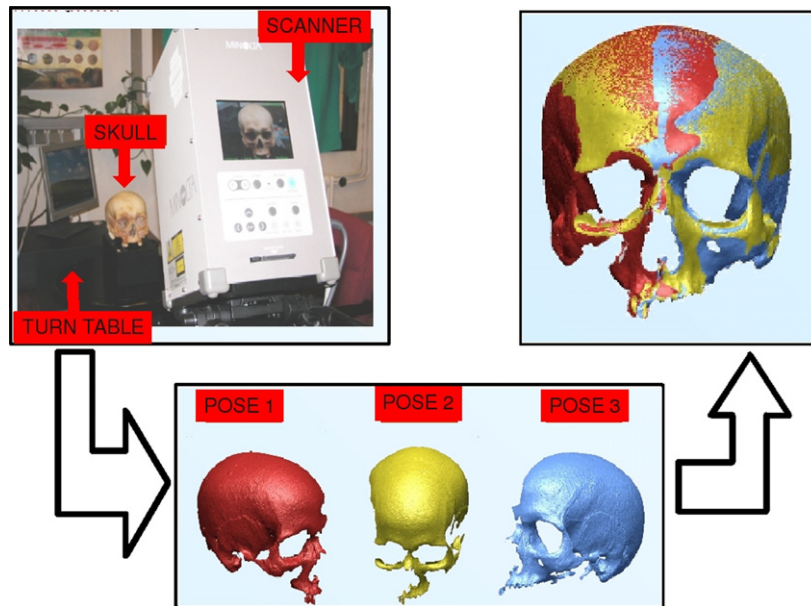**Fig. 1.** The IR optimization process.

Fig. 2. The 3D modeling procedure of forensic objects.

particular, we consider *crest-lines* as salient features [37,38] from 3D meshes of range images [39] in our feature-based IR approach.

3. Evolutionary IR methods

This section presents the development of the EIR research field in the last decades. To do so, Section 3.1 provides some basics on EC. Then, Section 3.2 is devoted to the description of the first EIR methods and their most important strengths and pitfalls. Finally, the state-of-the-art EIR methods are presented in Section 3.3.

3.1. Evolutionary computation

An extensive survey on every aspect related to the EC paradigm is out of the scope of this contribution. Interested readers will find a plenty of references reviewing this field [12,40–42]. Nevertheless, we would like to briefly describe the key concepts of EC in order to achieve a better understanding of the basis of EIR.

Evolutionary computation (EC) [12] uses computational models of evolutionary processes to evolve populations of solutions as key elements in the design and implementation of computer-based problem solving systems. EC is thus included into a wider family of advanced heuristic search and optimization algorithms called *metaheuristics* [43,44]. EC approaches constitute a very interesting choice since they are able to achieve good quality outcomes when global solutions of hard problems cannot be found with a reasonable amount of computational effort, for instance.

There is a variety of EC models that have been proposed and studied, which are referred as EAs [12]. Among them we refer to four well-defined EAs which have served as the basis for much of the activity in the field: genetic algorithms (GAs) [45,46], evolution strategies (ES) [47], genetic programming (GP) [48], and evolutionary programming (EP) [49].

In particular, GAs are probably the most used EAs in the literature to face real-world optimization problems. Some other EAs have been proposed in the last few years improving the state of the art on this field by adopting more suitable optimization strategies: CHC algorithm[1] [50,51], differential evolution (DE) [52,53],

memetic algorithms (MAs) [54], and scatter search (SS) [55], among others [42]. Moreover, other EC-based optimization algorithms following different evolutionary models have also been recently proposed such as estimation distribution algorithms (EDAs) [56] and particle swarm optimization (PSO) [57,58].

3.2. First evolutionary IR methods

The application of EAs to the IR optimization process has caused an outstanding interest in the last few decades. Unlike traditional ICP-based IR approaches, evolutionary ones need neither rough nor near-optimal prealignment of the images to proceed. Thus, they have become a more robust alternative to tackle complex IR problems. Fig. 3 depicts the evolution of the interest of the scientific community in this sort of approaches.[2]

Thanks to the global optimization nature of EAs, they aim to solve the drawbacks described by the ICP-based schemes (see Section 2). The first attempts to solve IR using EC approaches can be found in the eighties. The size of data as well as the number of parameters that are looked for prevent from an exhaustive search of the solutions. An approach based on a GA was proposed in 1984 for the 2D case and applied to angiography images [17]. Later, in 1989, Mandava et al. [59] used a 64-bit structure to represent a possible solution when trying to find the eight parameters of a bilinear transformation through a binary GA. Brunnström and Stoddart [60] proposed a new method based on the manual prealignment of range images followed by an automatic IR process using a novel GA that searches for solutions following the matching-based approach. Tsang [61] used 48-bit chromosomes to encode three test points as a base for the estimation of the 2D affine registration function by means of a binary-coded GA. In the case of Yamany et al. [33] and Chalermwat et al. [62], the same binary coding is found when dealing with 3D and 2D rigid transformations, respectively. Yamany et al. enforced a range of ±31° over the angles of rotation and ±127 units in displacement by defining a 42-bit chromosome with eight bits for each translation parameter

---

[1] The CHC acronym stands for: Cross generational elitist selection, Heterogeneous recombination, Cataclysmic mutation.

[2] The graphs in Fig. 3 were directly obtained from Thomson Reuter's Web of Science using the query *(Title OR Topic) ="(image AND (registration OR alignment OR matching) AND (evolution ∗ OR swarm OR chc OR neural OR scatter OR annealing OR tabu OR genetic))"*.
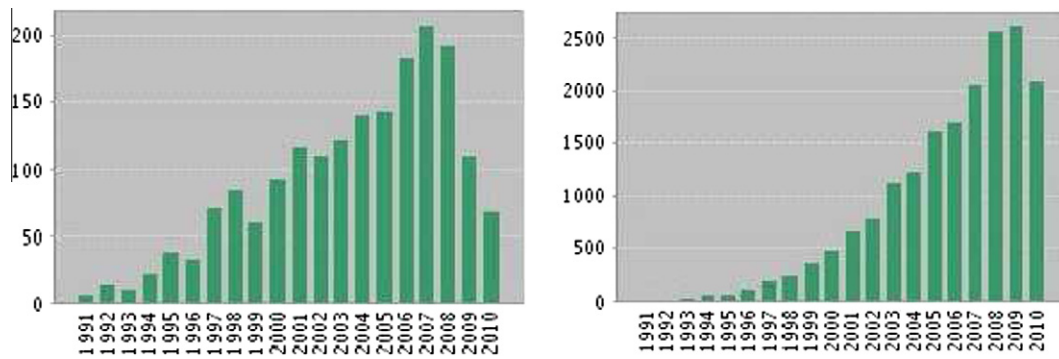
Fig. 3. Scientific production (left) and citations (right) in EIR. Query date: September, 2010.

and six bits for each rotation angle. Meanwhile, Chalermwat et al. used twelve bits for the coding of the 2D rotation parameter to get a search scope of ±20.48°, therefore allowing the use of a precision factor for the discretization of the continuous rotation angle interval. Other ten bits stored each of the two translation parameters (±512 pixels).

All the latter approaches showed several pitfalls from an EC perspective. They make use of the basic binary coding to solve inherently real coded problems, when it is well known that binary coding suffers from discretization flaws (as problem solutions of search space never visited) and requires transformations to real values for each solution evaluation. Moreover, the kind of GA considered is usually based on the old-fashioned original proposal by Holland [45,63], also named canonical GA (cGA). In this way, a selection strategy based on fitness-proportionate selection probability assignment and the stochastic sampling with replacement, as well as the classical one-point crossover and simple bit flipping mutation, are used. On the one hand, it is well known that such selection strategy causes a strong selective pressure, thus having a high risk of premature convergence of the algorithm. On the other hand, it has also been demonstrated that it is difficult for the single-point crossover to create useful descendants as it is excessively disruptive with respect to the building blocks [45]. Hence, the consideration of that old genetic framework is a clear pitfall affecting the latter group of proposals.

3.3. State-of-the-art evolutionary IR methods

In the last two decades, an important number of EC and meta-heuristic-based IR methods have been proposed to overcome the pitfalls described in the previous section. Table 1 summarizes the state of the art on EC and metaheuristic-based IR methods proposed to date. First column identifies both the reference and the year of publication of the algorithm. Second column refers to the coding scheme of solutions: R (real coding), B (binary coding), and I (integer coding). The third column concerns to the IR approach followed: P stands for a parameter-based approach while M stands for a matching-based approach. The optimization technique considered is shown in the fourth column. The family such technique belongs to, either a metaheuristic (MH) or an evolutionary (EA) approach, is also included in brackets in the fourth column. The main application, image modality, and computer architecture are reported in columns five, six, and seven, respectively.

Next, we analyze in deep and chronologically those EIR methods based on the use of more sophisticated evolutionary approaches solving the said drawbacks. All of them will be considered in our later experimental study. In our modest opinion, they are the outstanding EIR methods proposed in the last few years.

3.3.1. He and Narayana's GA-based proposal

This IR method [19] is a slight improvement of the previously reviewed Yamany et al.'s approach [33]. It considers a real coding scheme that makes use of arithmetic crossover and uniform mutation operators within an elitist generational model including a restart mechanism. This EIR method deals with rigid transformations following a two-step technique. First, a coarse parameter estimation is faced using a real-coded GA. Then, the obtained preliminary solution is refined by means of a local search procedure based on the dividing rectangle method. In the coarse resolution, the ranges of the parameters were set to: ±20 voxels along x and y directions, and ±40 voxels along z direction for the translation, and rotations of ±10° around x and y axes, and ±20° around z axis. However, the setting of the parameters range as well as the use of a simple rigid transformation between both images may be a weak point when trying to apply this method to some real-world environments.

3.3.2. Chow et al.'s GA-based proposal

The authors proposed the same generational and proportionate-fitness models for population reproduction than the latter method, but they introduced the use of a crossover operator that randomly selects the number of genes to be swapped [21]. The value to be accumulated for a mutated gene is generated randomly within a constant range for the rotation genes and dynamically computed for the translation ones according to the fitness value of the chromosome. They also make use of a GA with more suitable components to the current EC framework such as a real coding scheme and a sophisticated restart mechanism (named "dynamic boundary"). In spite of these improvements, there are some drawbacks in terms of accuracy, due to the fact that the authors work with a smaller, randomly selected data set from scene images with a huge amount of data. Besides, although the algorithm aims to get a quick registration estimation with the latter procedure, the efficiency could be reduced since it needs to perform a sort operation for each evaluation of the fitness function. As many of the mentioned proposals, it also has the limitation of only considering a rigid transformation (translation and rotation). Finally, the restart scheme assumes that, prior to its application, the population will fall in a search space region that includes or is near to the global optimum, which could be not always the case.

3.3.3. Wachowiak et al.'s PSO-based proposal

The authors contributed with a broad study on the performance of particle swarm optimization (PSO) [57,58] algorithms for solving the IR problem in biomedical applications [22]. In particular, they consider registering single slices (2D images) of 3D volumes to whole 3D volumes of medical images. Unlike typical EAs exploiting the competitive characteristics of biological evolution (e.g., survival of the fittest), PSO exploits cooperative and social aspects,

such as fish schooling, birds flocking, and insects swarming [73,74]. However, both evolutionary and PSO approaches are considered population-based schemes. In particular, PSO algorithms start with a random population called swarm of individuals or particles. After every iteration, they change their location in the search space guided by a velocity vector. The authors addressed the IR problem from the parameter-based approach, considering a rigid transformation and the mutual information (MI) [75] as similarity metric to be maximized. The variant called *PSO7* is the one achieving the best performance. It refers to a basic PSO the velocity vector update as follows:

$$v_i(t) = \chi[v_i(t-1) + \varphi_1 \mu_1(p_i - x_i(t-1)) + \varphi_2 \mu_2(g - x_i(t-1))] \tag{4}$$

where the optimization parameters take values $\kappa = 1.0$, $\varphi_1 = 2.1$, $\varphi_2 = 1.3$, and the constriction coefficient $\chi = 0.7298$.

Finally, the performance of the method depends on the initial orientation of the images to be registered. An adequate initialization must be provided by the user.

3.3.4. Silva et al.'s GA-based proposal

This method [23,32] addressed the pair-wise IR problem of range images acquired by 3D laser range scanners. The authors tackled the problem from the parameter-based approach for rigid transformations. The proposed approach is inspired in the steady-state evolutionary scheme of GAs (90% of the worst solutions are replaced instead of the entire population as done in generational schemes) [76]. Tournament selection, uniform crossover and random selection mutation operators are considered. Moreover, a hill-climbing algorithm is added to the GA in order to achieve more accurate results. This hybrid GA performs two well-defined pair-wise IR steps:

- Firstly, a coarse prealignment IR stage is accomplished by minimizing an objective function that makes use of a robust metric (initially proposed for image segmentation problems) based on Euclidean distances [77]. This stage takes 90% of the total computation time of the whole method, i.e. first and second stages.
- Next, a final refinement stage is performed during the remaining 10% of runtime. The previous coarser objective function is replaced by a new one that should be maximized. That function is called *surface inter-penetration measure* (SIM) and is given by:

$$SIM_{(A,B)} = \frac{|C_{(A,B)}|}{|A|}, \tag{5}$$

$$C_{(A,B)} = \{p \in A \,|[(q_i - c)n_c][(q_j - c)n_c] < 0\} \tag{6}$$

where A and B are the scene and the model images, respectively; q_i, q_j are two of the $N_p = 25$ closest scene points around the considered $p \in A$ scene point; c is the closest model point; and n_c is its normal vector.

The SIM metric reveals that more discriminating and accurate results can be obtained compared to those results achieved by metrics based on the Euclidean distances. However, the refinement stage using the SIM assumes that the results achieved during the prealignment stage will be really close to the global IR solution and that is not always the case. Indeed, the range of parameter values along the refinement stage is only ±5° for rotation and ±3 for translation from the optimal result achieved during the prealignment. Furthermore, another important drawback of this metric is the high computation time needed to evaluate it.

The authors used and extended this hybrid GA method to deal with the multiview IR problem, increasing the dimensionality of

the solutions [78]. They used several range datasets obtained from the SAMPL public-access database,[3] each one considering adjacent range images acquired every 20 rotation degrees of the turn table. The higher the degree of rotation, the lower the amount of overlapping existing between the images.

3.3.5. Lomonosov et al.'s GA-based proposal

Authors proposed a new method for the pair-wise IR problem of range images [24]. They considered the parameter-based approach using rigid transformations. The main novelties of this contribution are the inclusion of a degree of overlapping parameter in the solution vector and the utilization of the trimmed squares metric as objective function to be minimized. They constitute a different schematic approach for the IR problem that offers correct coarse IR results at overlaps under 50%. A random sampling procedure is tackled in order to speed up the performance of the method. The trimmed ICP variant (TrICP) is proposed as a fine-tuning method.

The method is based on a generational GA performing search in the seven dimensional space formed by three translation parameters, three rotation parameters, and the newly added degree of overlapping parameter. Authors used an integer coding representation of solutions which should be properly normalized onto the corresponding real-value range. Simple one-point crossover was employed and two mutation operators were introduced. Shift mutation alters one parameter randomly by a value not exceeding a 10% of the parameter range. Meanwhile, replacement mutation substitutes a parameter with a random value. Tournament and elitism were also employed. The authors dealt with three real-world noisy measured datasets provided by their REPLICA laser range scanner system and another two from the SAMPL public database. Nevertheless, the considered datasets include adjacent images acquired with up to 40° of rotation. Thus, the overlapping region of the adjacent images considered was always above the 50%. Hence, their assumption about the good performance provided by the trimmed squared metric considering overlapping regions below the 50% of the images is not sufficiently demonstrated.

3.3.6. Cordón et al.'s CHC-based proposal

This contribution used the sophisticated CHC EA adapted to the parameter-based approach that showed a very good intensification/diversification trade-off for the registration of MRIs [26]. Authors introduced two different variants of the method. First, they made use of binary-coded solutions and the HUX crossover [67], taking the original CHC structure as a base [50,51]. The second variant of the CHC-based IR method extends the latter structure to work in a real-coded fashion by considering a real to binary coding translation mechanism as well as using different specific real-coded genetic operators as the BLX-α crossover. Authors considered similarity transformations (rigid transformations with uniform scaling) for 3D medical IR. Therefore, eight-dimensional real coded solutions were considered to encode the similarity transformation (four parameters for rotation, three for translation, and one for uniform scaling). The fitness function is that one considered by the authors in their previous proposal [25] using the GCP data structure in order to tackle these particular scenarios.

3.3.7. De Falco et al.'s DE-based proposal

Authors proposed a new IR method based on the DE EA [27]. DE is a parallel direct search method that has proved to be a promising candidate to solve real-valued optimization problems [52,53]. DE combines simple arithmetic operators with the classical crossover,

---

[3] They were acquired with a Konica-Minolta Vivid 700© laser scanner. Resource available at http://sampl.eng.ohio-state.edu

mutation, and selection genetic operators within an easy to implement scheme. It shows the advantage of considering few control parameters, named mutation factor (F) and recombination rate (CR). The fundamental idea of DE is a new scheme for generating trial solutions by adding the weighted differenced vector between two population members to a third one. The proposed method is applied to two 2D IR problems: mosaicking and changes in time of satellite images. Registration is carried out from the parameter-based approach searching for the most suitable affine transformation (given by eleven real-coded parameters) in terms of maximization of the MI similarity metric.

3.3.8. Cordón et al.'s SS-based proposal

This IR method is based on the SS EA and adopts a matching-based approach [71]. Hence, a combinatorial optimization problem is tackled. It exploits problem dependent information by taking into account the curvature information extracted from MR and CT images. Unlike the typical randomized combination of solutions of GAs, the main idea behind SS [55,79] is a systematic combination between solutions taken from a considerably reduced evolved pool named *Reference Set* (RefSet). Indeed, the RefSet is usually between five and ten times lower than usual GA population sizes). The authors proposed new designs for three of the five SS components—the generator of diverse solutions, and both the improvement and the combination methods—to develop a proposal with improved performance compared with the state of the art methods following the matching-based approach. In particular, they succeeded at dealing with significant transformations between the two registered images, one of the ICP's pitfalls (see Section 2).

The main novelty of this feature-based IR method is that the heuristic values of the features are used to guide the matching. In particular, it exploits the information relative to local curvature characterizing the set of crest-lines points [37,38] extracted as relevant features of the scene and model images. Thus, the authors propose an advanced coding scheme where a given point matching is represented as a permutation. Besides, they define a function $m_{error}(\cdot)$ evaluating the goodness of the matching stored in a given solution, π, by using the said curvature values:

$$m_{error}(\pi) = \Delta k_1 + \Delta k_2 \text{ where } \Delta k_j = \sum_{i=1}^{r}(k_j^i - k_j^{\pi_i})^2, \; j = \{1, 2\} \quad (7)$$

Δk_1 and Δk_2 measure the error related to the matching of scene and model points with different values for the first and second principal curvatures, respectively.

Meanwhile, the objective function of this IR method will include both information regarding the usual IR measure $g(\pi)$ (MSE of the registration transformation resulting from the point matching encoded in π) and the previous criterion as follows:

$$\min \; F(\pi) = w_1 \cdot g(\pi) + w_2 \cdot m_{error}(\pi) \quad (8)$$

where w_1, w_2 are weighting coefficients defining the relative importance of each term.

3.3.9. Santamaría et al.'s SS-based proposal

In [28], the authors proposed different memetic-based IR methods to tackle a real-world application focused on the 3D reconstruction of forensic objects [69]. The parameter-based approach was used with seven-dimensional real-coded individuals encoding the rigid transformation (four parameters for rotation and three for translation). The similarity metric given by the objective function is:

$$F(I_s, I_m; f) = Median(d_i^2) = Median(\|f(p_i) - q_{cl}\|^2) \quad (9)$$

where $Median()$ corresponds to the computation of the median values of point-to-point squared Euclidean distances, d_i^2, between the

$N_{i_s}^{th}$ transformed scene points, $f(p_i)$, and their model closest points, q_{cl}. The GCP data structure is used in order to speed up the computation of the closest point rule.

The authors performed a broad study about the performance capabilities of different memetic-based IR methods. MAs are the result of the conjunction of the global search capabilities of EAs and the local search (LS) behavior of other *low-cost* heuristic procedures [54,80]. They considered three existing EA-based IR methods as the baseline algorithm: SS [25], CHC [26], and DE-based [27] IR methods (see the previous subsections for their respective description). For each of the previous three techniques, they considered the use of several LS algorithms (XLS [81], Solis and Wets [82], and Powell [83]) as improvement method within an embedded approach. The obtained experimental results in the 3D reconstruction of different human skull models, supported by a complementary non-parametric statistical test, revealed that the SS variant that made use of the deterministic LS application criterion and the XLS LS algorithm offered the best performance among all the developed memetic-based IR methods. It also outperformed the authors' previous methods based on the CHC and SS algorithms [25,26].

4. Experimental study

In this section we aim to develop an experimental study on the performance of the EIR methods described in Section 3. Salvi et al. made a deep study on the accuracy of the IR results in [5] tackling range IR problem instances. However, among the methods they reviewed and compared, only three are based on EC. Moreover, we aim to extend the performance analysis drawing our attention to the robustness of the methods, instead of constraining the study to the most accurate results.

As mentioned in Section 3, only the most sophisticated EIR methods in Table 1 will be included in the current experimental study. The selection of these advanced EIR methods was guided by two main criteria. On the one hand, our experimental study should not be biased by a particular evolutionary technique. Thus, we include different evolutionary approaches in order to represent the wide variety of techniques within the EC paradigm. On the other hand, when parameter-based and matching-based approaches are found in the literature for an evolutionary technique considered in our study, both approaches will be represented by at least one method. For benchmarking purposes, our study includes an IR method based on the classical ICP algorithm proposed by Liu [10] (named Liu-ICP), an extended ICP variant based on its hybridization with simulated annealing [65] (named Luck-ICP+SA), and an advanced method exploiting the capabilities of the iterated local search metaheuristic following a matching-based approach [68] (named Cordón-ILS). In summary, the considered methods are reviewed as follows (see Section 3 for a description of the EIR approaches):

- GAs:
  - *Parameter-based* approaches: Yamany-GA_{Binary} [33], He-*GA* [19], Chow-*GA* [21], Lomonosov-*GA* [24], Silva-*GA* [23].
  - *Matching-based* approaches: they are not considered in this study.[4]
- Other EAs:
  - *Parameter-based* approaches: Wachowiak-*PSO* [22], Cordón-CHC_{Binary} [67], Cordón-*CHC* [26], DeFalco-*DE* [27], Santamaría-*SS* [28].
  - *Matching-based* approach: Cordón-*SS* [71].

---

[4] Up to our knowledge, the proposal by Brunnström and Stoddart [60] is the only EIR method that could be classified in this category. However, we could obtain neither the code from the authors nor a detailed description of the GA in order to implement it on our own.

Table 1
Evolutionary and metaheuristic-based IR methods reviewed. See text for a detailed explanation.

Algorithm Refs.	Year	Representation			Search space		Optimization technique	Application field	Image modality	Computer architecture
		R	B	I	P	M				
[17]	1984		✔		✔		cGA (EA)	Medical imaging	2D	Serial
[59]	1989		✔		✔		cGA (EA)	Medical imaging	2D	Serial
[64]	1995		✔		✔		cGA (EA)	Medical imaging	3D	Serial
[60]	1996			✔		✔	GA (EA)	Reverse engineering	3D	Serial
[61]	1997		✔		✔		cGA (EA)	Non-specific	2D	Serial
[33]	1999		✔		✔		cGA (EA)	Medical imaging	3D	Serial
[18]	2000	✔			✔	✔	GA (EA)	Medical imaging	3D	Serial
[65]	2000	✔			✔	✔	ICP+SA (MH)	Modeling	3D	Serial
[62]	2001		✔		✔		GA (EA)	Remote sensing	2D	Parallel
[66]	2001	✔			✔		TS (MH)	Medical imaging	2D/3D	Serial
[19]	2002	✔			✔		GA (EA)	Medical imaging	3D	Serial
[20]	2002	✔			✔		GA (EA)	Modeling	3D	Parallel
[67]	2003		✔		✔		CHC (EA)	Medical imaging	3D	Serial
[21]	2004	✔			✔		GA (EA)	Modeling	3D	Serial
[22]	2004	✔			✔		PSO (EA)	Medical imaging	2D/3D	Serial
[23]	2005	✔			✔		HGA (EA)	Modeling	3D	Serial
[32]	2005	✔			✔		MOGA (EA)	Modeling	3D	Serial
[24]	2006	✔			✔		GA (EA)	Modeling	3D	Serial
[68]	2006			✔		✔	ILS (MH)	Medical imaging	3D	Serial
[25]	2006	✔			✔		SS (EA)	Medical imaging	3D	Serial
[26]	2006	✔			✔		CHC (EA)	Medical imaging	3D	Serial
[69]	2007	✔			✔		SS (EA)	Modeling	3D	Serial
[70]	2007		✔		✔		GA (EA)	Remote sensing	2D	Serial
[27]	2008	✔			✔		DE (EA)	Mosaicking	2D	Serial
[71]	2008			✔	✔	✔	SS (EA)	Medical imaging	3D	Serial
[28]	2009	✔			✔		SS (EA)	Modeling	3D	Serial
[72]	2009	✔			✔		SA (MH)	Face Recognition	3D	Serial

- Other metaheuristics and hybrids:
  - *Parameter-based* approach: Luck-*ICP + SA* [65].
  - *Matching-based* approach: Cordón-*ILS* [68].

Every method in the previous list demonstrated an outstanding behavior tackling a particular application field. Nevertheless, we aim to compare the performance of these methods and that is only possible when they tackle the same problem. Therefore, our experimental study is based on a real-world 3D modeling application all the selected methods will deal with.

Those fourteen IR methods are implemented in C++ and compiled with GNU/g++. We use a computer with an Intel Pentium IV 2.6 MHz processor and 2GB RAM.

We consider the parameter values proposed by the authors in their contributions. Nevertheless, we adapt the majority of the methods by using the same transformation (f) and objective function (see Eq. 3 in Section 2) in order to accomplish a fair comparison. The only exceptions to the latter are Cordón-*ILS* and Cordón-*SS* IR methods because their specific objective function designs are strongly interrelated to the structure of the optimization algorithms. Thus, we maintain their original objective functions.

As said in Section 2, a feature-based IR approach is considered [1,3]. We use a 3D crest line algorithm [39] to obtain feature points from 3D meshes of range images. These preprocessed images are the ones that will be used by every IR method to estimate the registration transformation. Once the IR method has finished, the original raw images are considered to measure the quality of the final results as follows:

$$RMSE = \sqrt{\frac{\sum_{i=1}^{r} ||f'(\vec{x}_i) - \vec{x}_i'||^2}{r}} \qquad (10)$$

where $f'(\vec{x}_i)$ refers to the ith point of the scene image transformed by the estimated rigid transformation f', r is the scene image size, and $\vec{x}_i'$ is the latter $\vec{x}_i$ scene point placed in its ground-truth location provided by using a properly calibrated mechanical device like a turn table (see Fig. 2 in Section 2).

In many real-world applications ground-truth locations are not available and the quality of the final solution to the IR problem cannot be evaluated. That is not the case of the current experimental study. Thus, the evaluation procedure in Eq. (10) allows us to accomplish a more reliable analysis of the performance of the methods under study.[5]

Fig. 4 illustrates the evaluation procedure. The left-hand picture refers to the ground-truth image (the I_1 range image of the SK(1) dataset introduced in Section 4.1) and the other two show the IR estimation obtained in two different runs of Yamany-GA_{Binary} [33] method. In particular, the worst result (middle picture) has a RMSE value of 13.7 cm while that associated to the last image takes value 5.3 cm. Notice that, these error values measure the distances from the ground-truth position of each point to its location estimated by the method under study (Yamany-GA_{Binary} in our example). The right most picture also shows three *a posteriori* known matchings and each correspondence links a transformed scene point and its ground truth position in the model ($f'(\vec{x}_i)$ and $\vec{x}_i'$, respectively). These are three of the r correspondences that contribute to the computation of the registration error in Eq. (10).

4.1. Range image datasets

The Physical Anthropology Lab of the University of Granada (Spain) provided us with three different range image datasets: two human skulls and one human teeth[6] named SK(1), SK(2) and TH, respectively. Skull SK(1) corresponds to a pathological case whose dimensions are clearly larger than usual (see Fig. 5). These forensic objects were acquired using a Konica-Minolta© 3D Laser Scanner VI-910 using a 640 × 480 image resolution, 8 μm precision,

---

[5] The final evaluation of the IR results is completely different to the evaluation of IR solutions performed within the iterative optimization procedure. Therein no information about the ground-truth solution is taken into account and every transformed point of the scene is paired with its nearest neighbor in the model.

[6] These are not public datasets because of the Spanish law for the protection of personal data.
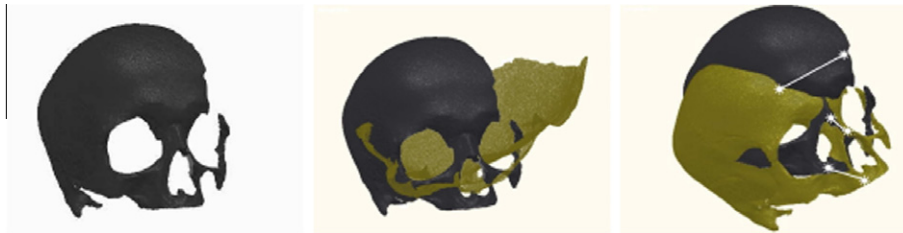
Fig. 4. From left to right: the ground-truth image and two independent runs of the Yamany's IR method. The right-most picture shows three known matchings between the ground-truth and the estimated images.
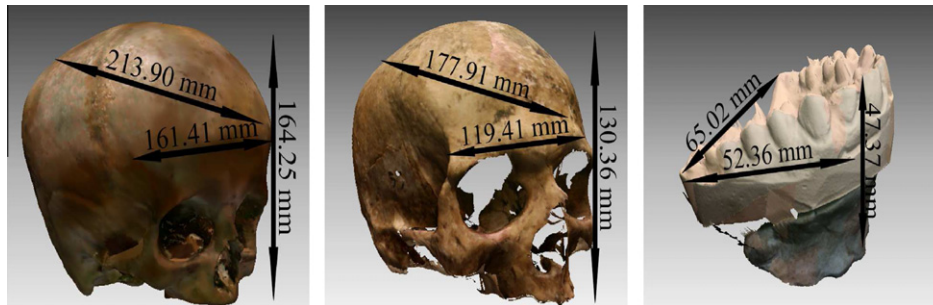

Fig. 5. From left to right: dimensions of the three forensic objects considered. Two human skulls and a human teeth.

and the middle lens of 14 mm. The scanner was also equipped with a mechanical turn table for precise alignment of the images. As said, the turn table gives us the chance to obtain a near optimal IR result that we will consider as the ground-truth 3D model for each dataset. The acquired images comprise around one hundred thousand points each. In order to ease the work of the forensic experts, we have taken into account important factors related to the scanning process like time and storage demand.[7] We consider two different rotation degrees of the turn table for acquisition purposes. In particular, the skulls were scanned every 45°. Meanwhile the views of the human teeth were acquired every 60° (see Fig. 6). The higher the rotation value the lower the overlapping area of adjacent range images, becoming a more complex IR problem. In the literature, these rotation values are considered the upper bounds of any IR method aiming to guarantee an acceptable result.

In order to follow a feature-based IR approach, we use a preprocessing algorithm that accomplishes the extraction of feature points from the range images by applying a 3D crest lines edge detector [39]. The resulting datasets consist of approximately one thousand points (see Table 2). Fig. 6 depicts one range image of every dataset (*SK*(1), *SK*(2), and *TH*) together with the extracted crest-line points.

4.2. Experimental design

The experimental design addresses six different pair-wise IR scenarios. For the sake of simplicity, we have selected three representative adjacent range images of each dataset (*SK*(1), *SK*(2), and *TH*). They lead us to tackle two pair-wise IR problem instances in each dataset. Given the sequence of adjacent range images I_1, I_2, and I_3, the said problem instances are defined by pairs of images $\{I_1, I_2\}$ and $\{I_3, I_2\}$. Notice that I_2 is the model image in both problem instances. Thus, the estimated transformations should be applied to the scene images ($\{I_1, I_3\}$). As said, ground-truth locations are available for every pair-wise IR problem instance.

On the other hand, the experimental design we consider is inspired by those ill-conditioned situations where forensic anthropologists are only able to reconstruct an optimal 3D model manually [28]. This situation is mainly motivated by the non existence of a mechanical device for scanner guidance, e.g. turn tables. Thus, we aim to simulate an unsupervised scanning process where there is no turn table available or the particular environment does not allow the forensic experts to use it. Such situations are simulated in each of the designed IR problem instance by generating random transformations applied to the ground-truth range images. Those random transformations should be estimated by every IR method. In particular, for each of the six problem instances tackled by the fourteen IR methods, 30 different runs are performed. Every run considers a different random rigid transformation. Every rigid transformation is randomly generated as follows: each of the three rotation axis parameters will be in the range $[-1, 1]$; the rotation angle will range in $[0°, 360°]$; and the range of three translation parameters is $[-40 \text{ mm}, 40 \text{ mm}]$. After a preliminary study, we noticed that twenty seconds was a suitable stop criterion to let all the algorithms converge properly.[8] In order to perform a fair comparison among the methods included in this study, we considered CPU time as the stop criterion. To our mind, that is the best choice because we aim to compare the performance of methods with heterogeneous designs. Different time limits were tested and 20 s was determined as a good threshold allowing the methods to achieve accurate solutions.

Finally, we adopt the usual two stage pair-wise IR approach [32]. It consists of a prealignment algorithm that provides coarse results, and a final refinement step that slightly adjusts them. Every EIR method is used for the prealignment step and one ICP-based IR algorithm is considered for the refinement.[9] Since the success of ICP-based IR methods highly depends on the initial estimation, it is important to note that the result provided by the

---

[7] Notice that the Physical Anthropology Lab of the University of Granada is willing to digitize hundreds of skulls and other skeletal remains.

[8] We tested all the IR methods from 5 to 20 s and noticed how the gain of performance from 15 to 20 s is not significant.

[9] A detailed explanation of the refinement stage is out of the scope of this survey. The interested reader is referred to [84].
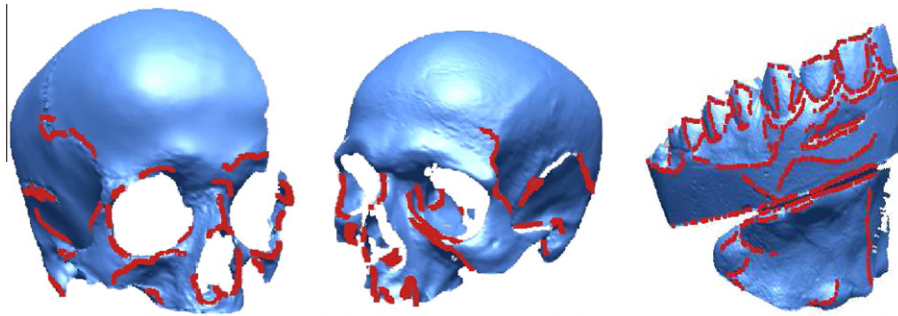
Fig. 6. From left to right: one of the three range images of each dataset $SK(1)$, $SK(2)$, and TH. Extracted crest-lines are drawn.

Table 2
Number of points in every image before and after applying the crest line algorithm.

	$SK(1)$			$SK(2)$			TH		
	I_1	I_2	I_3	I_1	I_2	I_3	I_1	I_2	I_3
Original	76794	68751	91590	116617	98139	118288	59033	62240	61345
Crest lines	1181	986	1322	2106	1995	2066	1160	1387	1175

prealignment algorithm will be crucial to achieve an accurate 3D model of the forensic object.

4.3. Analysis of results

Tables 3–5 show statistical results of the RMSE corresponding to the 30 runs of the different IR scenarios. In particular, each entry of these tables refer to the minimum, mean, and standard devia-

tion (in brackets) RMSE values. In each table, an additional column is added in order to average the performance of the prealignment stage. Thus, $SK(1)(I_1 - I_2)$ and $SK(1)(I_3 - I_2)$ RMSE values are averaged in the last column of Table 3. $SK(2)(I_1 - I_2)$ and $SK(2)(I_3 - I_2)$ RMSE values are averaged in the last column of Table 4. Finally, $TH(I_1 - I_2)$ and $TH(I_3 - I_2)$ RMSE values are averaged in the last column of Table 5. The unit length of the data included in these tables is millimeters.

Table 3
IR results of the skull image dataset $SK(1)$. Each entry corresponds to the minimum (top), mean (bottom), and standard deviation (in brackets) RMSE values obtained from the 30 different runs. The unit length is millimeters. The best minimum prealignment value and the best averaged mean prealignment value are in bold.

Code	IR method – search space	$SK(1)(I_1 - I_2)$		$SK(1)(I_3 - I_2)$		Average
		Prealignment	Refinement	Prealignment	Refinement	
ICP-based IR method						
A1	Liu-*ICP* [10]	12.63	–	48.90	–	30.77
	Matching-based approach	82.19 (±52.76)	–	96.88 (±44.14)	–	89.54 (±7.35)
Other metaheuristic-based IR methods						
B1	Luck-*ICP* + *SA*[65]	4.46	0.51	49.08	44.42	26.77
	Matching-based approach	82.69(±59.85)	93.49(±53.09)	101.26(±44.68)	107.82(±38.73)	91.98(±9.29)
B2	Cordón-*ILS*[68]	73.55	73.55	55.51	55.51	64.53
	Matching-based approach	116.56(±34.26)	116.56(±34.26)	126.68(±29.23)	126.68(±29.23)	121.62(±5.06)
EIR methods						
C1	Yamany-GA_{Binary}[33]	3.70	0.26	12.39	6.11	8.05
	Parameter-based approach	30.53(±30.86)	16.31 (±30.87)	42.78 (±29.35)	40.33 (±29.82)	36.66 (±6.13)
C2	He-*GA* [19]	3.06	0.16	8.69	2.08	5.88
	Parameter-based approach	8.97 (±3.63)	1.65 (±1.28)	24.79 (±16.06)	22.69 (±17.75)	16.88 (±7.91)
C3	Cordón-CHC_{Binary}[67]	3.52	0.20	8.84	6.56	6.18
	Parameter-based approach	29.01(±29.34)	22.28 (±31.92)	41.62 (±22.89)	39.75 (±24.13)	35.32(±6.31)
C4	Chow-*GA* [21]	6.57	0.27	10.84	4.36	8.71
	Parameter-based approach	28.03(±14.95)	18.47 (±17.97)	48.14 (±19.84)	44.65 (±22.12)	38.09 (±10.06)
C5	Wachowiak-*PSO* [22]	4.53	0.18	**2.98**	1.65	**3.76**
	Parameter-based approach	21.42 (±11.75)	10.86 (±13.76)	29.40 (±27.28)	25.82 (±28.28)	25.41 (±4)
C6	Silva-*GA* [23]	4.21	0.16	8.61	6.39	6.41
	Parameter-based approach	27.99 (±24.16)	14.23 (±25.60)	38.81(±20.92)	35.97(±23.80)	33.4(±5.41)
C7	Cordón-*CHC*[26]	4.24	0.31	11.46	9.72	7.85
	Parameter-based approach	10.83 (±11.45)	3.84 (±10.64)	32.41 (±19)	29.74 (±19.17)	21.62 (±10.79)
C8	Lomonosov-*GA* [24]	**1.90**	0.21	7.53	2	4.72
	Parameter-based approach	10.63(±5.13)	2.24(±2.70)	22.81(±13.45)	19.74(±14.33)	16.72(±6.09)
C9	Cordón-*SS* [71]	68.59	68.59	54.92	54.92	61.76
	Matching-based approach	78.23(±3.86)	78.23(±3.86)	88.89(±42.83)	88.89(±42.83)	83.56(±5.33)
C10	DeFalco-*DE*[27]	3.94	0.15	9.65	7.06	6.80
	Parameter-based approach	9.29(±2.91)	1.94(±1.01)	27.78(±27.67)	25.15(±28.08)	18.54(±9.25)
C11	Santamaría-*SS*[28]	3.28	0.20	8.12	5.39	5.7
	Parameter-based approach	*8.20(±2.68)*	1.73 (±0.98)	*18.79(±6.02)*	16.53(±6.34)	*13.50(±5.30)*

Numbers marked using bold font remark the best performance.

Table 4
IR results of the skull image dataset *SK*(2). Each entry corresponds to the minimum (top), mean (bottom), and standard deviation (in brackets) RMSE values obtained from the 30 different runs. The unit length is millimeters. The best minimum prealignment value and the best averaged mean prealignment value are in bold.

Code	IR method – search space	**SK**(2)($I_1 - I_2$)		**SK**(2)($I_3 - I_2$)		Average
		Prealignment	Refinement	Prealignment	Refinement	
ICP-based IR method						
A1	Liu-*ICP*[10]	11.95	–	14.47	–	13.21
	Matching-based approach	61.85(±37.39)	–	68.36 (±38.29)	–	65.11(±3.26)
Other metaheuristic-based IR methods						
B1	Luck-*ICP + SA*[65]	4.18	1.01	4.76	1.06	4.47
	Matching-based approach	53.74(±45.06)	58.92(±40.69)	66.92(±45.24)	72.34(±42.83)	60.33(±6.60)
B2	Cordón-*ILS*[68]	39.26	39.26	48.07	48.07	43.67
	Matching-based approach	75.49(±20.93)	75.49(±20.93)	81.71(±26.52)	81.71(±26.52)	78.60(±3.11)
EIR methods						
C1	Yamany-*GA*$_{Binary}$[33]	4.26	0.43	4.11	0.91	4.19
	Parameter-based approach	38.85(±32.72)	36.81(±34.23)	40.41(±39.40)	37.87(±41.02)	39.63(±0.61)
C2	He-*GA*[19]	5.03	0.57	3	0.92	4.02
	Parameter-based approach	17.57(±23.65)	10.53(±25.69)	*11.28*(±18.70)	6.16(±19.36)	14.43 (±3.15)
C3	Cordón-*CHC*$_{Binary}$[67]	5.21	0.68	2.23	0.92	3.72
	Parameter-based approach	36.15(±35.23)	33.29(±37.43)	36.58(±39.02)	33.59(±40.66)	36.37(±0.22)
C4	Chow-*GA*[21]	5.92	0.81	6.47	2.08	6.20
	Parameter-based approach	43.65(±34.72)	41.65(±35.95)	52.23(±41.53)	50.06(±42.84)	47.94(±4.29)
C5	Wachowiak-*PSO*[22]	5.48	0.93	3.12	0.93	4.30
	Parameter-based approach	38.42(±28.08)	36.42(±29.35)	36.21(±35.32)	31.76(±37.74)	37.32(±)
C6	Silva-*GA*[23]	5.54	0.63	2.85	0.91	4.20
	Parameter-based approach	31.62(±23.47)	20.81(±28.03)	33.90(±32.54)	28.66(±35.63)	32.76(±1.14)
C7	Cordón-*CHC* [26]	4.68	0.48	3.56	1.14	4.12
	Parameter-based approach	23.20(±27.01)	18.90(±29.17)	21.18(±33.83)	18.13(±35)	22.19(±1.06)
C8	Lomonosov-*GA*[24]	**3.23**	0.41	**1.93**	0.92	**2.58**
	Parameter-based approach	20.39(±17.24)	17.22(±18.51)	24.65(±30.11)	20.34(±31.91)	22.52(±2.13)
C9	Cordón-*SS*[71]	37.14	40	47.50	47.50	42.32
	Matching-based approach	40(±1.33)	40(±1.33)	52.47 (±3.71)	52.47(±3.71)	46.24(±6.24)
C10	DeFalco-*DE*[27]	4.35	0.42	3.82	0.98	4.09
	Parameter-based approach	13.15(±15.50)	8.18(±17.15)	13.84(±28.76)	9.66(±29.57)	13.50 (±0.35)
C11	Santamaría-*SS*[28]	4.66	0.73	3.17	1.04	3.92
	Parameter-based approach	*9*(±8.56)	3.36(±9.39)	8.69(±20.68)	5.27(±21.34)	*8.85*(±0.16)

Numbers marked using bold font remark the best performance.

Table 5
IR results of the teeth image dataset *TH*. Each entry corresponds to the minimum (top), mean (bottom), and standard deviation (in brackets) RMSE values obtained from the 30 different runs. The unit length is millimeters. The best minimum prealignment value and the best averaged mean prealignment value are in bold.

Code	IR method – search space	TH($I_1 - I_2$)		TH($I_3 - I_2$)		Average
		Prealignment	Refinement	Prealignment	Refinement	
ICP-based IR method						
1	Liu-*ICP*[10]	1.78	–	0.96	–	1.37
	Matching-based approach	24.52(±13.42)	–	25.20 (±15.57)	–	24.86(±0.34)
Other metaheuristic-based IR methods						
B1	Luck-*ICP + SA*[65]	0.76	0.63	1.08	0.85	0.92
	Matching-based approach	24.97(±13.31)	25.71(±12.45)	22.95(±17.29)	24.04(±15.85)	23.96(±1.01)
B2	Cordón-*ILS*[68]	20.12	20.12	22.93	22.93	21.53
	Matching-based approach	33.53(±4.59)	33.53(±4.59)	31.22(±4.56)	31.22(±4.56)	32.38(±1.16)
EIR methods						
C1	Yamany-*GA*$_{Binary}$ [33]	**0.37**	0.59	1.10	0.5	**0.74**
	Parameter-based approach	22.08(±15.84)	21.81(±16.16)	14.72(±15.61)	14.19(±15.95)	18.40(±3.68)
C2	He-*GA*[19]	0.76	0.60	0.90	0.46	0.83
	Parameter-based approach	18.50(±17.10)	18(±17.55)	16.24(±16.91)	15.53(±17.43)	17.37(±0.82)
C3	Cordón-*CHC*$_{Binary}$[67]	0.84	0.54	1.17	0.68	1.01
	Parameter-based approach	18.79(±15.09)	18.57(±15.33)	20.69(±17.32)	20.10(±17.85)	19.74(±0.95)
C4	Chow-*GA*[21]	11.80	11.49	3.91	2.61	2.86
	Parameter-based approach	32.05(±9.44)	31.97(±9.51)	37.54(±11.70)	37.47(±11.94)	34.80(±2.75)
C5	Wachowiak-*PSO*[22]	0.82	0.58	**0.73**	0.43	0.78
	Parameter-based approach	22.92(±15.97)	22.64(±16.29)	21.85(±18.32)	21.42(±18.79)	22.39(±0.29)
C6	Silva-*GA*[23]	0.77	0.57	0.95	0.61	0.86
	Parameter-based approach	22.20(±14.04)	22.02(±14.30)	17.76(±15.90)	17.39(±16.23)	19.98(±2.13)
C7	Cordón-*CHC*[26]	0.78	0.60	1.12	0.70	0.95
	Parameter-based approach	19.91(±17.21)	19.82(±17.30)	17.44(±17.49)	17.21(±17.67)	18.68(±1.24)
C8	Lomonosov-*GA*[24]	1.28	0.57	0.86	0.46	1.07
	Parameter-based approach	17.99(±16.28)	17.34 (±16.86)	14.26(±17.47)	13.03(±18.18)	16.13 (±1.87)
C9	Cordón-*SS*[71]	19.72	19.72	32.93	32.93	26.33
	Matching-based approach	24.94(±6.36)	24.94(±6.36)	33.32(±0.23)	33.32(±0.23)	29.13(±4.19)
C10	DeFalco-*DE*[27]	0.79	0.58	1.10	0.51	0.95
	Parameter-based approach	*10.63*(±16.25)	10.36 (±16.40)	12.26(±16.39)	11.84(±16.65)	*11.45* (±0.82)
C11	Santamaría-*SS*[28]	0.60	0.60	1.08	0.66	0.84
	Parameter-based approach	15.70(±18.18)	15.57(±18.25)	*9.11*(±15.46)	8.75(±15.58)	12.41 (±3.30)

Numbers marked using bold font remark the best performance.

On the one hand, we aim to analyze the robustness of the methods facing the prealignment stage of the six IR problems considered (see Tables 3–5 and Appendix A). On the other hand, we aim to compare the performance of the methods. Figs. 7–9 show
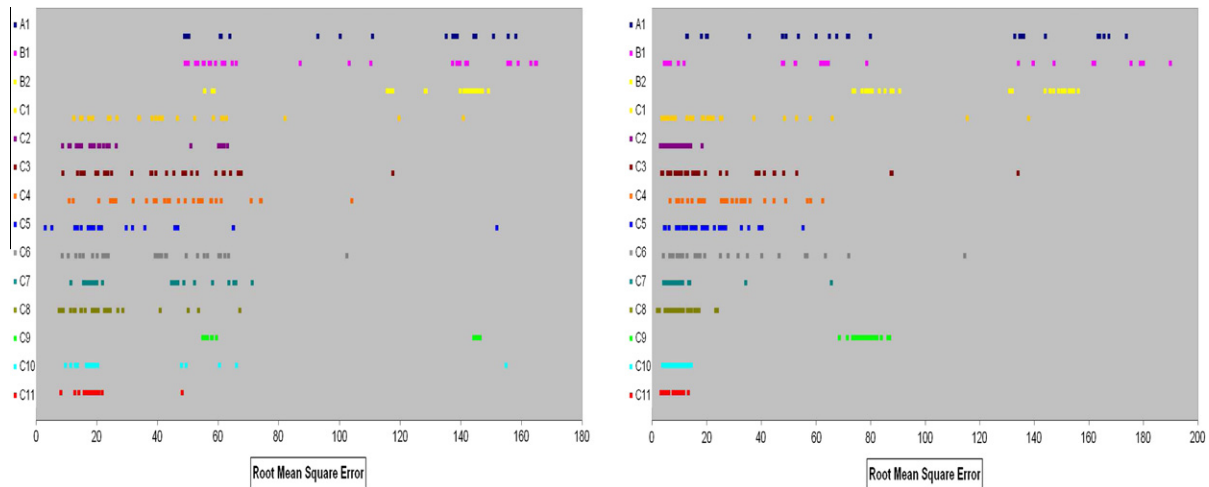

Fig. 7. From left to right, RMSE distribution corresponding to the 30 runs of the IR problems SK(1)($I_1 - I_2$) and SK(1)($I_3 - I_2$).
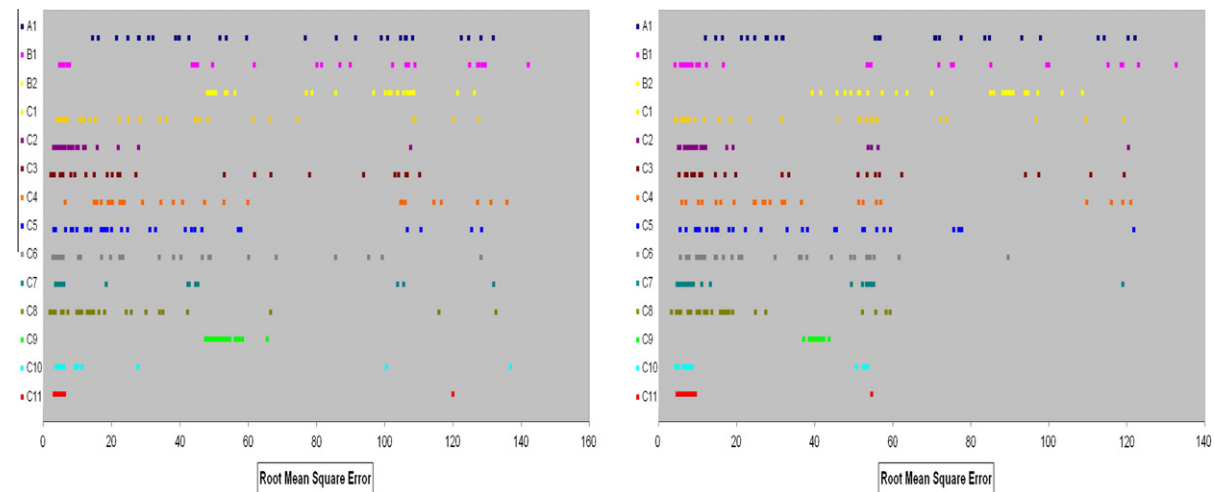

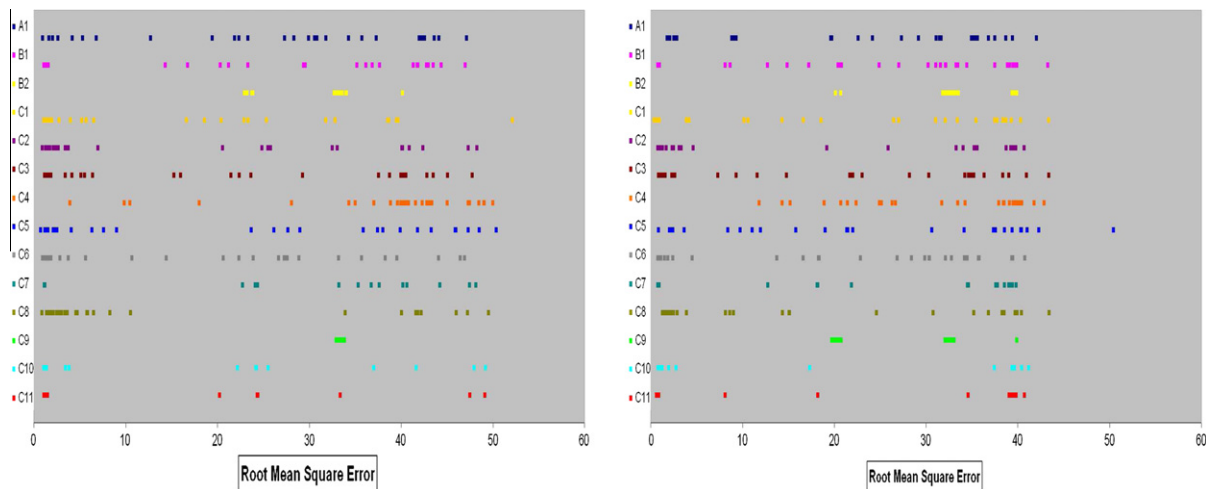**Fig. 8.** From left to right, RMSE distribution corresponding to the 30 runs of the IR problems SK(2)($I_1 - I_2$) and SK(2)($I_3 - I_2$).

Fig. 9. From left to right, RMSE distribution corresponding to the 30 runs of the IR problems TH($I_1 - I_2$) and TH($I_3 - I_2$).
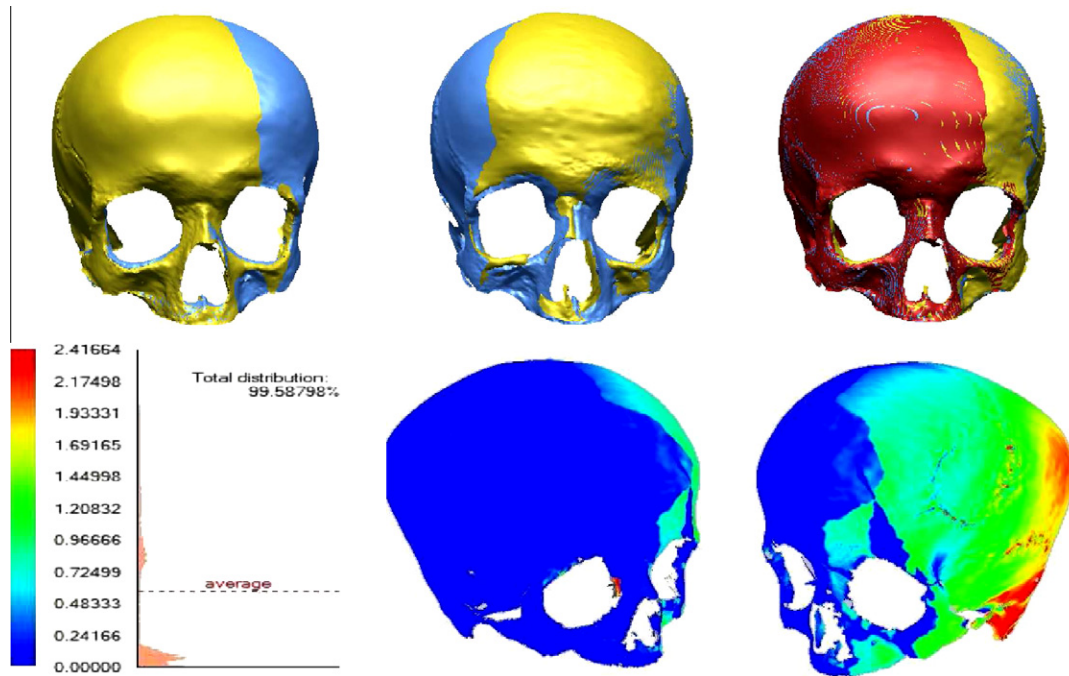
Fig. 10. Summary of the most remarkable results. From left to right: the top row shows the best two (pair-wise) prealignment IR results obtained by Wachowiak-*PSO* (C5) and the reconstruction result (combining the previous two prealignments) of SK(1) after refinement. The bottom row depicts the distance deviation histogram comparing the latter reconstruction result and the ground-truth 3D model.
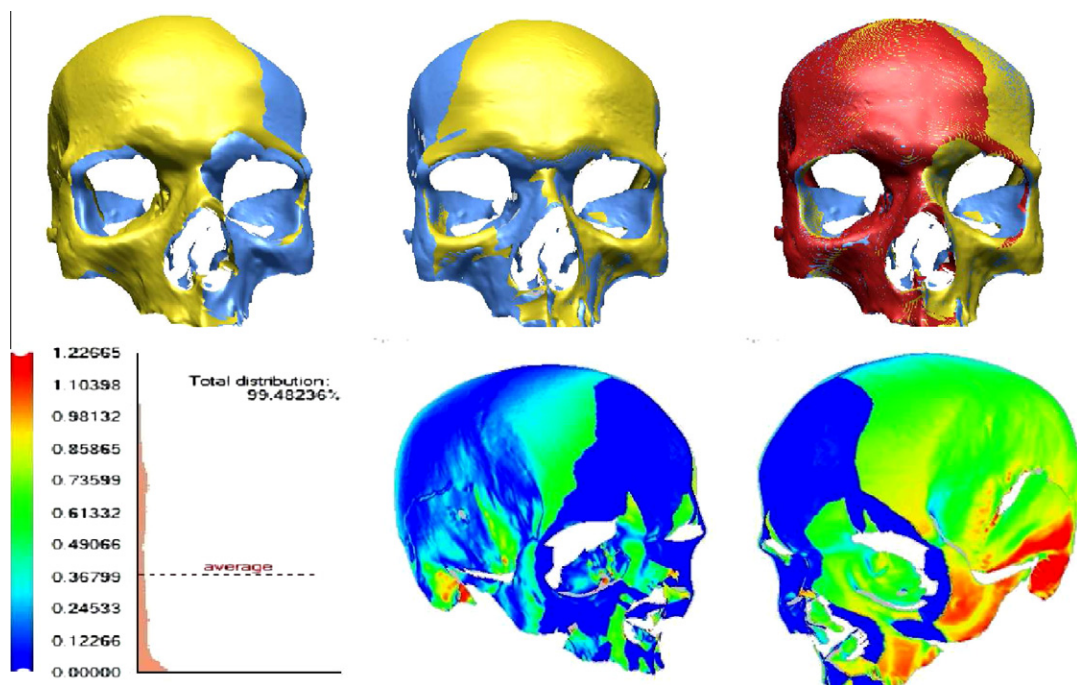

Fig. 11. Summary of the most remarkable results. From left to right: the top row shows the best two (pair-wise) prealignment IR results obtained by Silva-*GA* (C6) and the reconstruction result (combining the previous two prealignments) of SK(2) after refinement. The bottom row depicts the distance deviation histogram comparing the latter reconstruction result and the ground-truth 3D model.

the RMSE distribution corresponding to the 30 runs of the two IR problems tackled to achieve the 3D models related to the *SK*(1), *SK*(2), and *TH* datasets, respectively.

The following three conclusions can be drawn according to the robustness of every IR method facing the prealignment stage in the six IR scenarios:

- All the matching-based methods but Cordón-SS (C9) are characterized by their low robustness: Liu-ICP (A1), Luck-*ICP + SA* (B1), and Cordón-ILS (B2).
- Differences in robustness between the matching-based and the parameter-based IR approaches are significant. The latter demonstrate the best behavior.
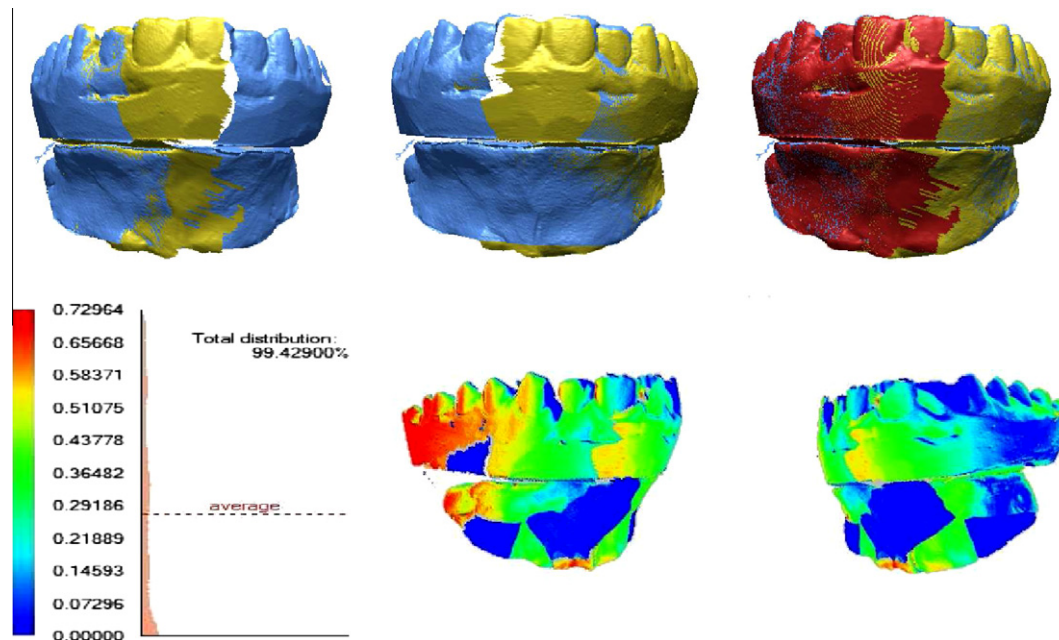
Fig. 12. Summary of the most remarkable results. From left to right: the top row shows the best two (pair-wise) prealignment IR results obtained by Cordón-*CHC* (C7) and the reconstruction result (combining the previous two prealignments) of TH after refinement. The bottom row depicts the distance deviation histogram comparing the latter reconstruction result and the ground-truth 3D model.

- The most complex IR problem considered is the teeth (*TH*). Since that image dataset was acquired considering a higher rotation angle of the turn table, the size of the overlapping region between adjacent acquisitions was smaller. Thus, the complexity of the IR problem is increased. Nevertheless, DeFalco-DE (C10) and Santamaría-SS (C11) IR methods also maintain their high robustness in this problem instance.

From the results depicted in Figs. 7–9 we can highlight that the majority of the EIR methods following a parameter-based approach achieve the best and the most robust performance along the 30 different runs. In particular, the four best IR methods facing the three IR scenarios are: Santamaría-SS (C11), DeFalco-DE (C10), He-GA (C2), and Lomonosov-GA (C8). Real-coded EIR methods obtain the best results. Figs. 10–12 depict some of the more relevant IR results for the three IR scenarios considered.

We also noticed the poor performance obtained by the matching-based methods. Among them, Cordón-SS (C9) provides the best results.

In general, all the EIR methods considered but Liu-ICP (A1), Luck-*ICP + SA* (B1), Cordón-ILS (B2), and Cordón-SS (C9) achieve accurate results in at least two of the three IR scenarios. The accuracy of the four latter methods is significantly low according to the minimum RMSE value in Tables 3–5.

Santamaría-SS (C11), Wachowiak-PSO (C5), He-GA (C2), and Lomonosov-GA (C8) are the most accurate EIR methods. As said, we focused our analysis on the prealignment stage of the IR process. Nevertheless, if the solutions after prealignment are compared with those achieved after refinement using ICP-based methods, the importance of the prealignment stage is clearly shown. Indeed, the prealignment stage will not be affected by local optima only if the prealignment results are acceptable,[10] thus leading to high quality solutions (see Figs. 10–12).

5. Conclusions

IR is a very active research field. The large number of publications related to IR shows the high relevance of this topic in computer vision. In the last few decades, evolutionary approaches have demonstrated their ability to tackle the IR problem thanks to their robust behavior as global optimization techniques. Indeed, EIR methods own the capability to perform a robust search in complex search spaces. Unlike traditional IR methods as the ICP algorithm, EIR methods do not need a good initial estimation of the alignment to avoid local optima.

Several works review the state of the art in IR [1–5]. However, they include just a few of the important number of works that lay their foundations on EC [12]. With the aim of bridging this gap, we proposed a survey including, in our modest opinion, the outstanding evolutionary methods.

Furthermore, a broad experimentation considering a real-world application was accomplished in order to facilitate the comparison of the performance of the EIR methods. In particular, we faced the 3D modeling of forensic objects. The results demonstrate the good behavior of most of the EIR methods. They outperformed classical approaches based on the ICP algorithm. Specifically, the EIR methods considering a parameter-based approach provided the most robust and accurate results. However, there is no general method that is able to achieve the best results for all possible real-world problems as it is stated by the *No Free Lunch* theorem [85]. Hence, the selected method should always be adapted to the problem at hand. Finally, future works on EIR should focus on using advanced optimization strategies based on EC in order to improve the robustness and accuracy of the state of the art. Likewise, there is a need of new EIR approaches supplying improved capabilities regarding speeding up the computation time, e.g. by using general-purpose computing on graphics processing units (GPGPU) [86?].

---

[10] According to the rotation angle, a prealignment result can be considered acceptable when the error in the estimation of the rotation angle is ±5° [24,32].

and Dr. Alemán) for their support during the acquisition of the range images and the validation of the results.

Appendix A. Supplementary data

Supplementary data associated with this article can be found, in the on-line version of the journal, at ScienceDirect.com. Every available image shows a pair of box-plots depicting the performance of the IR methods tackling the two prealignment problems for each dataset (*SK*(1), *SK*(2) and *TH*). These box-plots are derived from the outcomes of the 30 runs summarized in Tables 3–5. Supplementary data associated with this article can be found, in the online version, at doi:10.1016/j.cviu.2011.05.006.

References

[1] L.G. Brown, A survey of image registration techniques, ACM Comput. Surv. 24 (4) (1992) 325–376.

[2] A. Goshtasby, 2D and 3D Image Registration, Wiley Interscience, 2005.

[3] B. Zitová, J. Flusser, Image registration methods: a survey, Image Vision Comput. 21 (2003) 977–1000.

[4] J.B. Maintz, M.A. Viergever, A survey of medical image registration, Med. Image Anal. 2 (1) (1998) 1–36.

[5] J. Salvi, C. Matabosch, D. Fofi, J. Forest, A review of recent range image registration methods with accuracy evaluation, Image Vision Comput. 25 (5) (2007) 578–596.

[6] P.J. Besl, N.D. McKay, A method for registration of 3D shapes, IEEE Trans. Pattern Anal. 14 (1992) 239–256.

[7] Y. Chen, G. Medioni, Object modelling by registration of multiple range images, Image Vision Comput. 10 (3) (1992) 145–155.

[8] S. Rusinkiewicz, M. Levoy, Efficient variants of the ICP algorithm, in: Third International Conference on 3D Digital Imaging and Modeling (3DIM'01), Quebec, Canada, 2001, pp. 145–152.

[9] G.C. Sharp, S.W. Lee, D.K. Wehe, ICP registration using invariant features, IEEE Trans. Pattern Anal. 24 (1) (2002) 90–102.

[10] Y. Liu, Improving ICP with easy implementation for free form surface matching, Pattern Recogn. 37 (2) (2004) 211–226.

[11] T. Masuda, Registration and integration of multiple range images by matching signed distance fields for object shape modeling, Comput. Vis. Image Understand. 87 (1-3) (2002) 51–65.

[12] T. Bäck, D.B. Fogel, Z. Michalewicz, Handbook of Evolutionary Computation, IOP Publishing Ltd. and Oxford University Press, 1997.

[13] G. Olague, S. Cagnoni, E. Lutton, Introduction to the special issue on evolutionary computer vision and image understanding, Pattern Recogn. Lett. 27 (11) (2006) 1161–1163.

[14] S. Cagnoni, E. Lutton, G. Olague, Editorial introduction to the special issue on evolutionary computer vision, Evolut. Comput. 16 (4) (2008) 437–438.

[15] M. Nachtegael, E. Kerre, S. Damas, D. Van der Weken, Special issue on recent advances in soft computing in image processing, Int. J. Approx. Reason. 50 (1) (2009) 1–2.

[16] T. Bäck, Evolutionary Algorithms in Theory and Practice: Evolution Strategies, Evolutionary Programming, Genetic Algorithms, Oxford University Press, 1996.

[17] J. Fitzpatrick, J. Grefenstette, D. Gucht, Image registration by genetic search, in: IEEE Southeast Conference, Louisville, EEUU, 1984, pp. 460–464.

[18] J.M. Rouet, J.J. Jacq, C. Roux, Genetic algorithms for a robust 3-D MR-CT registration, IEEE Trans. Inf. Technol. B. 4 (2) (2000) 126–136.

[19] R. He, P.A. Narayana, Global optimization of mutual information: application to three-dimensional retrospective registration of magnetic resonance images, Comput. Med. Imag. Grap. 26 (2002) 277–292.

[20] C. Robertson, R.B. Fisher, Parallel evolutionary registration of range data, Comput. Vis. Image Understand. 87 (2002) 39–50.

[21] C.K. Chow, H.T. Tsui, T. Lee, Surface registration using a dynamic genetic algorithm, Pattern Recogn. 37 (2004) 105–117.

[22] M.P. Wachowiak, R. Smolikova, Y. Zheng, J.M. Zurada, A.S. El-Maghraby, An approach to multimodal biomedical image registration utilizing particle swarm optimization, IEEE Trans. Evolut. Comput. 8 (3) (2004) 289–301.

[23] L. Silva, O.R.P. Bellon, K.L. Boyer, Precision range image registration using a robust surface interpenetration measure and enhanced genetic algorithms, IEEE Trans. Pattern Anal. 27 (5) (2005) 762–776.

[24] E. Lomonosov, D. Chetverikov, A. Ekart, Pre-registration of arbitrarily oriented 3D surfaces using a genetic algorithm, Pattern Recogn. Lett. 27 (11) (2006) 1201–1208.

[25] O. Cordón, S. Damas, J. Santamaría, A fast and accurate approach for 3D image registration using the scatter search evolutionary algorithm, Pattern Recogn. Lett. 27 (11) (2006) 1191–1200.

[26] O. Cordón, S. Damas, J. Santamaría, Feature-based image registration by means of the CHC evolutionary algorithm, Image Vis. Comput. 22 (2006) 525–533.

[27] I. De Falco, A. Della Cioppa, D. Maisto, E. Tarantino, Differential evolution as a viable tool for satellite image registration, Appl. Soft Comput. 8 (4) (2008) 1453–1462.

[28] J. Santamaría, O. Cordón, S. Damas, J. García-Torres, A. Quirin, Performance evaluation of memetic approaches in 3D reconstruction of forensic objects, Soft Comput. 13 (8-9) (2009) 883–904.

[29] R.J. Campbell, P.J. Flynn, A survey of free-form object representation and recognition techniques, Comput. Vis. Image Understand. 81 (2) (2001) 166–210.

[30] M. Rodrigues, R. Fisher, Y. Liu, Special issue on registration and fusion of range images, Comput. Vis. Image Underst. 87 (1-3) (2002) 1–7.

[31] G. Godin, P. Hebert, T. Masuda, G. Taubin, Special issue on new advances in 3D imaging and modeling, Comput. Vis. Image Understand. 113 (11) (2009) 1105–1180.

[32] L. Silva, O.R.P. Bellon, K.L. Boyer, Robust Range Image Registration using Genetic Algorithms and the Surface Interpenetration Measure, World Scientific, 2005.

[33] S.M. Yamany, M.N. Ahmed, A.A. Farag, A new genetic-based technique for matching 3D curves and surfaces, Pattern Recogn. 32 (1999) 1817–1820.

[34] P. Krsek, T. Pajdla, V. Hlavác, Differential invariants as the base of triangulated surface registration, Comput. Vis. Image Understand. 87 (1-3) (2002) 27–38.

[35] T. Masuda, Log-polar height maps for multiple range image registration, Comput. Vis. Image Understand. 113 (11) (2009) 1158–1169.

[36] J. Wyngaerd, L. Gool, Automatic crude patch registration: toward automatic 3D model building, Comput. Vis. Image Understand. 87 (1-3) (2002) 8–26.

[37] O. Monga, R. Deriche, G. Malandain, J.P. Cocquerez, Recursive filtering and edge tracking: two primary tools for 3D edge detection, Image Vis. Comput. 9 (4) (1991) 203–214.

[38] J.P. Thirion, A. Gourdon, Computing the differential characteristics of isointensity surfaces, Comput. Vis. Image Understand. 61 (2) (1995) 190–202.

[39] S. Yoshizawa, A. Belyaev, H.P. Seidel, Fast and robust detection of crest lines on meshes, in: SPM '05: Proceedings of the 2005 ACM Symposium on Solid and Physical Modeling, ACM Press, New York, NY, EEUU, 2005, pp. 227–232.

[40] K. De Jong, Evolutionary Computation, The MIT Press, 2002.

[41] A. Eiben, J. Smith, Introduction to Evolutionary Computation, Springer, Berlin, 2003.

[42] D. Fogel, Evolutionary Computation: Toward a New Philosophy of Machine Intelligence, Wiley IEEE Press, 2005.

[43] F. Glover, G.A. Kochenberger, Handbook of Metaheuristics, Kluwer Academic Publishers, 2003.

[44] F. Glover, Future paths for integer programming and links to artificial intelligence, Comput. Oper. Res. 13 (5) (1986) 533–549.

[45] D.E. Goldberg, Genetic Algoritms in Search and Optimization, Addison-Wesley, New York, EEUU, 1989.

[46] Z. Michalewicz, Genetic Algorithms + Data Structures = Evolution Programs, Springer, Verlag, 1996.

[47] H. Schwefel, Evolution and Optimum Seeking: The Sixth Generation, John Wiley & Sons, Inc., New York, NY, USA, 1993.

[48] J. Koza, Genetic Programming: On the Programming of Computers by Means of Natural Selection, The MIT Press, 1992.

[49] D. Fogel, System Identification through Simulated Evolution: A Machine Learning Approach to Modeling, Ginn Press, 1991.

[50] L.J. Eshelman, The CHC adaptive search algorithm: how to safe search when engaging in non traditional genetic recombination, in: G.J.E. Rawlins (Ed.), Foundations of Genetic Algorithms, vol. 1, Morgan Kaufmann, San Mateo, EEUU, 1991, pp. 265–283.

[51] L.J. Eshelman, J.D. Schaffer, Preventing premature convergence by preventing incest, in: R. Belew, L.B. Booker (Eds.), 4th International Conference on Genetic Algorithms, Morgan Kaufman, San Mateo, EEUU, 1991. pp. 115–122.

[52] K. Price, An introduction to differential evolution, in: D. Corne, M. Dorigo, F. Glover (Eds.), New Ideas in Optimization, McGraw-Hill, 1999, pp. 79–108.

[53] R. Storn, Differential evolution – a simple and efficient heuristic for global optimization over continuous spaces, J. Global Optim. 11 (4) (1997) 341–359.

[54] P. Moscato, On Evolution, Search, Optimization, Genetic Algorithms and Martial Arts: Towards Memetic Algorithms, Report 826, Caltech Concurrent Computation Program, Pasadena, California, 1989.

[55] M. Laguna, R. Martí, Scatter Search: Methodology and Implementations in C, Kluwer Academic Publishers, Boston, 2003.

[56] J.A. Lozano, P. Larrañaga, I. Inza, E. Bengoetxea, Towards a New Evolutionary Computation: Advances on Estimation of Distribution Algorithms, Springer, Verlag, 2006.

[57] M. Clerc, Particle Swarm Optimization, ISTE Publishing Company, 2006.

[58] J. Kennedy, R. Eberhart, Swarm Intelligence, Morgan Kaufmann, San Francisco, CA, 2001.

[59] V.R. Mandava, J.M. Fitzpatrick, D.R. Pickens, Adaptive search space scaling in digital image registration, IEEE Trans. Med. Imag. 8 (3) (1989) 251–262.

[60] K. Brunnström, A. Stoddart, Genetic algorithms for free-form surface matching, in: International Conference of Pattern Recognition, Vienna, Germany, 1996, pp. 689–693.

[61] P.W.M. Tsang, A genetic algorithm for aligning object shapes, Image Vis. Comput. 15 (1997) 819–831.

[62] P. Chalermwat, T. El-Ghazawi, J. LeMoigne, 2-phase GA-based image registration on parallel clusters, Future Gen. Comp. Syst. 17 (2001) 467–476.

[63] J.H. Holland, Adaptation in Natural and Artificial Systems, The University of Michigan Press, Ann Arbor, 1975.

[64] J. Jacq, C. Roux, Registration of 3-D images by genetic optimization, Pattern Recogn. Lett. 16 (8) (1995) 823–841.

[65] J.P. Luck, C.Q. Little, W. Hoff, Registration of range data using a hybrid simulated annealing and iterative closest point algorithm, in: IEEE

International Conference on Robotics and Automation (ICRA'00), 2000, pp. 3739–3744.

[66] M.P. Wachowiak, A.S. El-maghraby, The continuous tabu search as an optimizer for 2D-to-3D biomedical image registration, in: W. Niessen, M. Viergever (Eds.), 4th International Conference on Medical Image Computing and Computer-Assisted Intervention (MICCAI'01), Lecture Notes in Computer Science, vol. 2207, Springer, Berlin/Heidelberg, Utrecht, The Netherlands, 2001, pp. 1273–1274,.

[67] O. Cordón, S. Damas, J. Santamaría, A CHC evolutionary algorithm for 3D image registration, in: T. Bilgic, B.D. Baets, O. Bogazici (Eds.), International Fuzzy Systems Association World Congress (IFSA'03), Lecture Notes in Artificial Intelligence, vol. 2715, Springer-Verlag, Istambul, Turkey, 2003, pp. 404–411.

[68] O. Cordón, S. Damas, Image registration with iterated local search, J. Heuristics 12 (2006) 73–94.

[69] J. Santamaría, O. Cordón, S. Damas, I. Alemán, M. Botella, A Scatter search-based technique for pair-wise 3D range image registration in forensic anthropology, Soft Comput. 11 (2007) 819–828.

[70] G. Pascale, L. Troiano, A niche based genetic algorithm for image registration, in: Ninth International Conference on Enterprise Information Systems (ICEIS 2007), 2007, pp. 342–347.

[71] O. Cordón, S. Damas, J. Santamaría, R. Martí, Scatter search for the 3D point matching problem in image registration, INFORMS J. Comput. 20 (2008) 55–68.

[72] C. Queirolo, L. Silva, O. Bellon, M. Pamplona, 3D face recognition using simulated annealing and the surface interpenetration measure, IEEE Trans. Pattern Anal. 32 (2) (2010) 206–219.

[73] M. Clerc, J. Kennedy, The particle swarm – explosion, stability, and convergence in a multidimensional complex space, IEEE Trans. Evolut. Comput. 6 (1) (2002) 58–73.

[74] J. Kennedy, R. Eberhart, Particle swarm optimization, in: IEEE International Conference on Neural Networks, vol. 4, 1995, pp. 1942–1948.

[75] P. Viola, W.M. Wells, Alignment by maximization of mutual information, Int. J. Comput. Vis. 24 (1997) 137–154.

[76] Z. Michalewicz, C. Janikow, GENOCOP: a genetic algorithm for numerical optimization problems with linear constraints, Commun. ACM (1996) 175.

[77] P. Gotardo, O. Bellon, K. Boyer, L. Silva, Range image segmentation into planar and quadric surfaces using an improved robust estimator and genetic algorithm, IEEE Trans. Syst. Man Cyber. B 34 (6) (2004) 2303–2316.

[78] L. Silva, O.R.P. Bellon, K.L. Boyer, Multiview range image registration using the surface interpenetration measure, Image Vis. Comput. 25 (1) (2007) 114–125.

[79] F. Glover, Heuristic for integer programming using surrogate constraints, Decis. Sci. 8 (1977) 156–166.

[80] N. Krasnogor, J. Smith, A tutorial for competent memetic algorithms: model, taxonomy and design issues, IEEE Trans. Evolut. Comput. 9 (5) (2005) 474–488.

[81] H.G. Beyer, K. Deb, On self-adaptive features in real-parameter evolutionary algorithms, IEEE Trans. Evolut. Comput. 5 (3) (2001) 250–270.

[82] F.J. Solis, R.J.B. Wets, Minimization by random search techniques, Math. Oper. Res. 6 (1981) 19–30.

[83] M. Powell, An efficient method for finding the minimum of a function of several variables without calculating derivatives, Comput. J. 7 (1964) 155–162.

[84] G. Dalley, P. Flynn, Pair-wise range image registration: a study in outlier classification, Comput. Vis. Image Understand. 87 (1-3) (2002) 104–115.

[85] D.H. Wolpert, W.G. Macready, No free lunch theorems for search, Tech. Rep. SFI-TR-95-02-010, The Santa Fe Institute, 1996.

[86] H. Nguyen, GPU Gems 3, Addison-Wesley Professional, 2007.